RESEARCH REPORT OPEN ACCESS

Layer-Specific Connectivity and Functional Interference of Chrna2+ Layer 5 Martinotti Cells in the Primary Motor Cortex

Anna Velica[1] | Katharina Henriksson[1] | Thawann Malfatti[1] | Barbara Ciralli[1] | Ingrid Nogueira[2] | Evridiki Asimakidou[1,3] | Klas Kullander[1] [ID]

[1]Department of Immunology, Genetics and Pathology, Uppsala University, Uppsala, Sweden | [2]Brain Institute, Federal University of Rio Grande do Norte, Natal, RN, Brazil | [3]Department of Clinical Neurosciences, University of Cambridge, UK

Correspondence: Klas Kullander (klas.kullander@uu.se)

ABSTRACT

The cortical somatostatin interneuron population includes several diverse cell types, among them the Martinotti cells. Layer-specific differences in connectivity and function between different subtypes of Martinotti cells are becoming apparent, which require contemporary studies to investigate cortical interneurons in a layer and subtype-specific manner. In this study, we investigate the connectivity of a subtype of Chrna2+ layer 5 Martinotti cells in the primary motor cortex, using a monosynaptic retrograde rabies viral tracer. We found direct input from pyramidal cells and local parvalbumin interneurons. In addition, we found long-range direct inputs from the motor thalamus, substantia innominata of the basal forebrain, and globus pallidus. Based on the observed input pattern, we tested and found an increased number of falls in the hanging wire test upon temporary overexcitation of Chrna2+ layer 5 Martinotti cells, suggesting that Chrna2+ Martinotti cells in the motor cortex can interfere with sensorimotor integration. In summary, our study provides novel insights into the connectivity and functional role of Mα2 cells in the M1 forelimb area, highlighting their unique integration of local and long-range inputs critical for sensorimotor processing, which lay the groundwork for further exploration of their role in cortical plasticity and motor learning.

1 | Introduction

Cortical inhibitory interneurons shape pyramidal cell (PC) output and contribute significantly to circuit complexity (Markram et al. 2004). They are commonly grouped into four major subclasses based on their expression of parvalbumin (PV), somatostatin (SST), or the ionotropic serotonin receptor 5HT3a. Further, 5HT3a interneurons are grouped into vasoactive intestinal polypeptide (VIP) and non-VIP interneurons (Rudy et al. 2011; Tremblay et al. 2016). The SST interneuron population includes several diverse cell types like large basket cells, double-bouquet cells, long-range inhibitory projection cells, bitufted cells, fanning-out Martinotti cells, and T-shaped Martinotti cells (Markram et al. 2004; Muñoz et al. 2017; Riedemann 2019). Martinotti cells, which are found across cortical layer 2–6, send inhibitory projections to layer 1 where they target the distal dendrite of PCs that reside in deeper cortical layers (Wang et al. 2004). Genetic markers characterizing distinct subtypes of SST interneurons with similar morphology, projections patterns, electrophysiological properties, layer localization, and functional specificity have been identified over the past few years (Gouwens et al. 2020; Hilscher et al. 2017; Wu et al. 2023). It has been proposed that SST interneurons include up to a hundred distinct subtypes (Yavorska and Wehr 2016). In addition, there are clear layer-specific differences in connectivity and function (Gouwens et al. 2020; Muñoz et al. 2017; Wu et al. 2023; Xu et al. 2013), with layer-specific differences in cortical and thalamic input to SST interneurons (Okoro et al. 2022). Despite the increasing evidence for layer-specific heterogeneity, most studies still focus on the connectivity and function of PV, SST, and VIP interneurons as a whole, grouping several subtypes and cells across cortical layers. To extend our knowledge of how the brain processes information, the cortical connectome and functionality needs to be investigated in a layer and subtype-specific manner.

Previous studies have found that layer 5 Martinotti cells send inhibitory projections selectively to pyramidal tract PCs where they can reset and synchronize PC activity in a frequency-dependent manner (Hilscher et al. 2017; Wu et al. 2023). PC spikes control the firing of surrounding layer 5 Martinotti cells, and optogenetic activation of layer 5 Martinotti cells controlled by connected PCs results in synchronization of neighboring PC spike trains (Hilscher et al. 2017). These in vitro results suggest a role for Martinotti cells in regulating PC activity; however, the relation to other interneurons and possible in vivo functions is not yet clear. Here, we investigate the connectivity and function of a subset of Martinotti cells (herein referred to as $M^{\alpha 2}$ cells) located in cortical layer 5b, expressing the cholinergic receptor nicotinic alpha 2 subunit (Chrna2; Hilscher et al. 2017; Wu et al. 2023).

2 | Material and Methods

2.1 | Animals

All animal procedures were approved by the local animal research ethical committee (Uppsala djurförsöksetiska nämnd) and followed the Swedish Animal Welfare Act (Svensk författningssamling (SFS) 2018:1192), The Swedish Animal Welfare Ordinance (SFS 2019:66) and the Regulations and general advice for laboratory animals (SJVFS 2019:9, Saknr L 150). Ethical permit number: 5.8.18-08463/2018, 5.8.18-08464/2018, and 5.8.18-07526/2023. Chrna2-Cre mice, produced and bred in our own facility (Leão et al. 2012), were crossed with either C57BL/6J (Taconic, Denmark) or GT (ROSA)26Sortm1.1(CAG-EGFP)Fsh/Mmjax (RRID:MMRRC_032037-JAX, 14) mice and the offspring were genotyped and kept heterozygous. Primers: Chrna2-Cre 5′-gacagccattttctcgcttc-3′ (forward) and 5′-aggcaaattttggtgtacgg-3′ (reverse); EGFP 5′-gacgtaaacggccacaagttc-3′ (forward) and 5′-cttctcgttggggtctttgct-3′ (reverse). Animals were housed with littermates in approximately $501\,cm^2$ individually ventilated cages (up to five animals/cage) with bedding and enrichment, kept in a 12-h light on/light off cycle (6 a.m.–6 p.m.), maintained at $21 \pm 2°C$ with a humidity of 45–64% and provided food (diet pellets, Scanbur, Sweden) and tap water ad libitum. Mice were 6–25 weeks old. For tracing experiments, 14 mice (9 Chrna2-Cre[tg/wt], 1 Chrna2-Cre[tg/wt];EGFP:loxP[lx/wt], and 4 Chrna2-Cre[wt/wt]) of both sexes were used. For both behavioral experiments, 14 female mice were used (7 Chrna2-Cre[tg/wt] and 7 Chrna2-Cre[wt/wt]), respectively. Throughout the paper, control mice refer to Cre-negative littermates that have received the same treatment as Cre-positive mice.

2.2 | Surgery

Mice were anesthetized with 1–4% isoflurane (Baxter), 2 mg/kg bupivacaine (Marcain, AstraZeneca), 5 mg/kg carprofen (Norocarp vet, N-vet or Rimadyl Biovis vet), and 0.1 mg/kg buprenorphine (Vetergesic vet, Ceva) subcutaneously. The scalp was incised. Muscles and periosteum were removed using 3% hydrogen peroxide (Sigma-Aldrich). A hole (1 mm in diameter) was drilled (coordinates relative to bregma: AP 0.8 mm, ML 1.5 mm, and DV − 1.3 mm). Coordinates were chosen based on the Paxinos and Franklin atlas (Paxinos and Franklin 2012) as well as previous studies investigating the somatotopic organization of the motor cortex (Tennant et al. 2011; Wang et al. 2017). Viral vectors were injected using a 10 µL Nanofil Hamilton syringe (WPI, USA) mounted on a stereotaxic frame. Ten minutes post-injection, the needle was slowly withdrawn from the brain. The wound was stitched with resorbable sutures (Vicryl rapide, Ethicon, 6–0).

For tracing experiments, mice were injected unilaterally (right hemisphere) with 500 nL of AAV8-hSYN-FLEX-TVA-E66T-P2A-GFP-P2A-oG-WPRE (LOT BA-229a: viral titer 3.98×10^{12} VG/mL, LOT BA-229b: viral titer 7.20×10^{12} VG/mL, Charité, Germany, 15) and 7 days later with 500 nL of the ΔG-rabies virus, pseudotyped EnvA, mCherry (BRVEnvA-1o: viral titer: 1.00×10^8 VG/mL, BRVEnvA-1n: viral titer: 1.4×10^8 VG/mL, BRVEnvA-1s: viral titer 3.4×10^8 VG/mL, Charité, Germany). Speed of the injections: 100 nL/min. The animals were perfused 7 to 10 days after the last injection.

For the Hanging wire test, mice were injected bilaterally with 300 nL of AAV9-hSyn-DIO-hDM3q-mCherry (Addgene, LOT 44361-AAV9, viral titer 2.3×1013 GC/mL) or AAV8/hSyn-DIO-hM4D(Gi)-mCherry (Addgene, 44362-AAV9, LOT v162687, viral titer 2.20E+13 GC/mL; Krashes et al. 2011) diluted in 300 nL

sterile saline (9 mg/mL, Fresenius Kabi, Sweden) at a speed of 200 nL/min. pAAV-hSyn-DIO-hM3D(Gq)-mCherry and pAAV-hSyn-DIO-hM4D(Gi)-mCherry were a gift from Bryan Roth (Addgene plasmid #44361-AAV9; http://n2t.net/addgene:44361; RRID:Addgene_44361 and #44362-AAV8; http://n2t.net/addgene:44362; RRID:Addgene_44362). Viral transduction was confirmed by post hoc histological analysis.

2.3 | Tissue Preparation and Immunohistochemistry

Mice were transcardially perfused with phosphate buffered saline (PBS, Fisher Scientific, CAT 10051163) followed by 4% formaldehyde (VWR Chemicals BDH®, CAT 9713.1000) and brains were dissected. The brains were post-fixed in 4% formaldehyde overnight at 4°C, washed three times for 10 min in PBS and kept in PBS at 4°C until sectioning (a few hours or days). Sections of embedded brains (4% agarose in PBS) were cut at a thickness of 70 μm using a Vibratome (Leica VT1000S). For the tracing experiments, the entire brain was sectioned, mounted and examined in a widefield microscope (Olympus BX61WI, Japan) with a 10× objective. For control mice (Cre-negative littermates) and the first four Chrna2-Cre+ mice, all GFP and mCherry positive cells were imaged. For the following Chrna2-Cre+ mice used, the sections were checked in the widefield microscope with a 10× objective to find sections suitable for immunohistochemical and DAPI analysis. For the hanging wire experiments, the area around the injection site was sectioned and immunohistochemistry was performed on AAV9-hSyn-DIO-hDM3q-mCherry injected tissue to enhance the mCherry signal. Sections used for immunohistochemistry were pre-blocked for 1–2 h at room temperature in a blocking solution (3% donkey serum and 0.3% Triton®X in PBS), incubated overnight (anti-vasoactive intestinal polypeptide and anti-somatostatin were incubated for 72 h) at 4°C on a rocking table with the primary antibodies diluted in the blocking solution. Thereafter, sections were washed with PBS three times for 10 min, incubated for 3 h at room temperature with the corresponding secondary antibody diluted 1:500 in the blocking solution, stained with 200 ng/mL DAPI (VWR, CAT 40011) in PBS for 10 min, and washed two times for 10 min with PBS and mounted with ProLong™ Gold Antifade Mountant (ThermoFisher Scientific, CAT P10144) or Fluoroshield (Abcam, CAT ab104135) on glass slides (Superfrost®Plus, Thermo Scientific). In some cases, 200 ng/mL DAPI was added to the blocking solution during the secondary antibody incubation. Primary antibodies: anti-GFP (Abcam, ab13970, chicken polyclonal, dilution 1:1000), anti-parvalbumin (Swant, PV27, rabbit, dilution 1:1000), anti-calbindin (Swant, CB38, rabbit polyclonal, dilution 1:1000), anti-calretinin (Swant, CR7697, rabbit, dilution 1:1000, anti-choline acetyltransferase (Millipore, AB144P, goat, dilution 1:1000), anti-gamma-aminobutyric acid (GABA; Sigma, A2502, rabbit, dilution 1:750), anti-somatostatin (Merck Millipore, clone YC7, rat, dilution 1:150), anti-vasoactive intestinal peptide (ThermoFisher, PA5-78224, rabbit polyclonal, 1:1000), anti-mCherry (ThermoFisher, M11217, rat, dilution 1:1000). Secondary antibodies: goat anti-chicken A488 (Jackson ImmunoResearch 103-545-155), donkey anti-rabbit A647 (ThermoFisherScientific A32795), donkey anti-rabbit A647 (Invitrogen A31573), donkey anti-goat A647 (Invitrogen A21447), donkey anti-rat A647 (Invitrogen A48272), donkey anti-rat 488 (Invitrogen A21208).

2.4 | Imaging and Image Post Processing

Most wide field images were acquired on a Zeiss Axio Imager Z2 (Zeiss, Germany) with a 10× objective (effective NA 0.45), a colibri LED 7 and Zen blue software (Zeiss, Germany), using a multi-band bandpass filter (Zeiss, Germany) with the filter excitation wavelengths 370–400 nm, 450–488 nm, 540–570 nm, 614–647 nm, 720–750 nm and the filter emission wavelengths 412–438 nm, 501–527 nm, 582–601 nm, 662–700 nm, 770–800 nm for DAPI, Alexa 647, and GFP and a single-band bandpass filter (TxRed-4040C-ZHE-ZERO, Semrock) with the excitation wavelengths 540–552 nm and emission wavelengths 590–4095 nm for mCherry. LED-module 385 nm was used for DAPI, LED-module 630 nm for Alexa 647, LED-module 475 nm for GFP, and LED-module 567 nm for mCherry. Some images were taken using an Olympus BX61WI fluorescence microscope (Olympus, Japan) with a 10× (effective NA 0.40) objective and a Volocity 4.1.0 software (Quorum Technologies) or a Zeiss LSM700 confocal microscope (BioVis facility, Uppsala University). Brightness and contrast were adjusted in the Fiji software (Schindelin et al. 2012), equally for the whole image and without obscuring any data.

Coordinates were identified based on the Paxinos and Franklin atlas (Paxinos and Franklin 2012). Abbreviations and brain region identification followed the Allen brain atlas data portal (http://atlas.brain-map.org). Cell counts were done manually with the Fiji counter plugin and the cell diameter was measured manually in Fiji. For cortical layer counts DAPI was used to distinguish the layers. For calculating cell distance to cortex surface, two points were marked at the cortex surface, then a line was interpolated from these points for each coronal image, and cell dorsoventral (DV) coordinates were calculated as the shortest Euclidean distance between each cell and the interpolated line. For the visualization of cell distance to cortex surface, the traced cells were divided in three different groups; by the injection site (on brain sections with starter cells), anterior (>0.5 mm anterior of the most anterior starter cell) and posterior (> 0.1 mm posterior of the most posterior starter cell). The probability density function of cells was calculated by performing a bidimensional gaussian kernel density estimate on the cell coordinates (ML × AP or AP × DV) interpolated 100 points on each axis.

In the Chrna2Cre-EGFP mouse, there were seven Chrna2/GFP and mCherry double-positive cells, of which at least six were classified as starter cells based on their location in cortical layer 5 by the injection site and based on their extensive dendritic staining compared to the surrounding GFP labelled Chrna2+ cells, indicating that they had a higher GFP expression after being transfected with the GFP-expressing helper virus. One Chrna2/EGFP and mCherry double-positive cell was classified as a likely traced cell based on its location more than 1 mm away from the injection site.
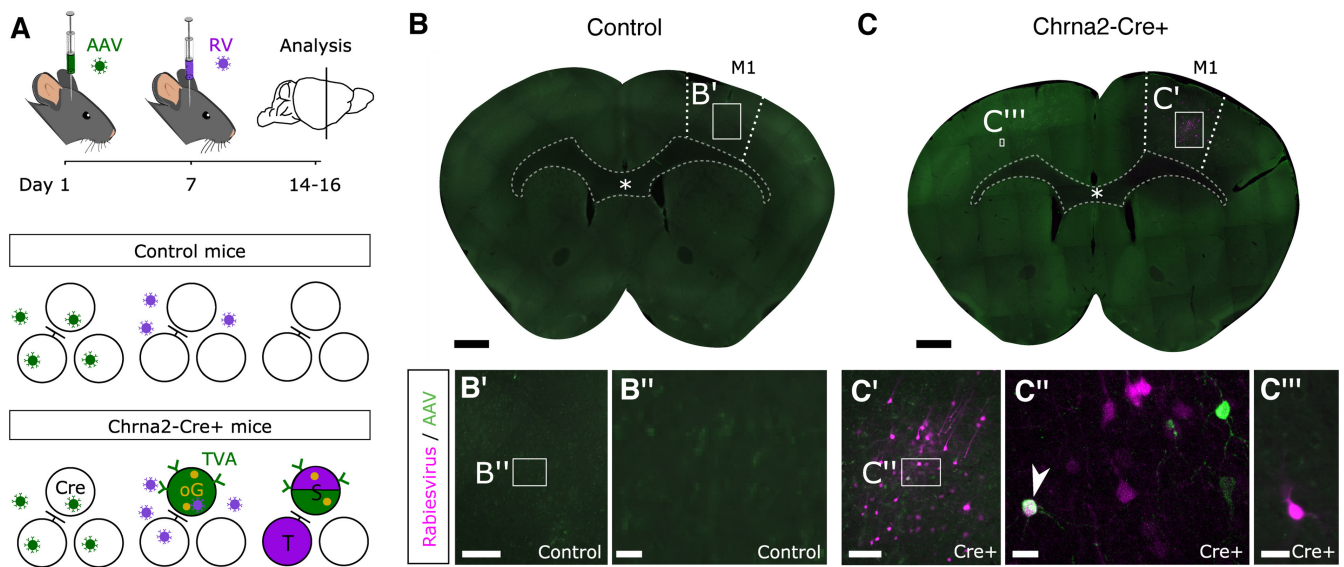
FIGURE 1 | Retrogradely traced inputs to $M^{\alpha 2}$ cells in the primary motor cortex (M1). (A) Schematic illustration of monosynaptic retrograde tracing using a G-protein deleted, EnvA coated rabies virus (RV). The vector carries a mCherry fluorescent marker and requires an avian tumor virus receptor A (TVA) receptor to enter cells and an optimized glycoprotein (oG protein) to retrogradely cross a synapse. The TVA receptor, oG protein and a green fluorescent protein (GFP) were delivered into the M1 by a Cre-dependent helper virus (AAV), 7 days prior to injection of the RV. Cells that are infected by both the AAV and RV are referred to as starter cells (S), while cells that are only infected by the RV are referred to as traced cells (T). (B,C) Images of brain sections at the injection site, with AAV infected cells (green) in cortical layer 5b, starter cells (white) and traced cells (magenta) found in Chrna2-Cre + mice (C) but not in control mice (B). Boxes indicate areas of enlargement seen in B′, C′ and C″. * = corpus callosum. Scale bars: 500 μm in B and C, 200 μm in B′, C′, 20 μm in C″ and 40 μm in C‴.

2.5 | Hanging Wire Test

Mice were tested four (hDM4i) or eight (hDM3q) weeks after viral vector injection. We routinely perform experiments 4–10 weeks post-injection and have not observed any differences in the expression levels or the functional responses of the DREADDs. In the first test session, all mice received 0.9% NaCl intraperitoneally 45 min before the test session started. During the test session, the mice were placed hanging from their forepaws on the middle of a wire, which was stretched between two posts 40 cm above the ground. During the 3-min test session, the mouse was re-placed on the wire each time it fell down. One (hDM4i) to 2 (hDM3q) weeks later, the mice received 0.01 mg/kg clozapine (Hello Bio, batch E0697-1-1) intraperitoneally 45 min before the test.

2.6 | Statistical Analysis

To account for the non-normal distribution of cell diameter data as determined by Shapiro's test, statistical analyses were performed using Kruskal-Wallis test with F-ratios (Gorsuch and Lehmann 2017). Post hoc pairwise comparisons were conducted using the Mann–Whitney U test, with multiple comparisons adjusted using the Holm method, as the comparisons were made between independent sets of cells. The effect of both genotype (Control vs. Chrna2-Cre+) and treatment (NaCl vs clozapine) on hanging wire falls was evaluated using mixed-models 2-way ANOVA for the hM3Dq dataset, and ANOVA-type statistics with F1-LD-F1 model (non-parametric equivalent of the mixed-models 2-way ANOVA (Noguchi et al. 2012) for the HM4Di dataset. For the hM3Dq dataset, post hoc pairwise comparisons

for genotype differences used Tukey's HSD test, and those for treatment differences used a paired t-test with Holm correction for multiple comparisons. For the hM4Di dataset, pairwise differences were evaluated with the Mann-Whitney U test for genotype, and the Wilcoxon signed-rank test for treatment. The significance level for statistical analyses was set at a false positive risk of $\alpha = 0.05$. Error bars in all figures represent the standard error of the mean (SEM), and the filled areas in violin plots represent the entire data range, with triangle markers denoting means.

3 | Results

Monosynaptic inputs to $M^{\alpha 2}$ cells, in the forelimb area of the primary motor cortex (M1; (Paxinos and Franklin 2012; Tennant et al. 2011; Wang et al. 2017), were investigated using a modified rabies viral vector combined with a helper virus (Hagendorf and Conzelmann 2015; Wickersham et al. 2007). Cells that were not infected by the helper virus but were labelled by the rabies virus are referred to as traced cells, whereas cells that were infected by both viruses are referred to as starter cells (Figure 1A). A flowchart for adequate control experiments was used to validate the viral tools (Velica and Kullander 2024). In control mice (Cre-negative littermates, $n = 4$), no helper virus infected cells were found, and only an average of one rabies virus infected cell was found by the injection site, with no rabies virus infected cells in distant brain regions (Figure 1B, Table 1). In Chrna2-Cre+ mice ($n = 4$), on average, 11 starter cells, infected by both the helper and rabies virus, were found by the injection site (Figure 1C, Table 1, $n = 3$ mice, average total number of traced cells = 799, $n = 4$).

TABLE 1 | Summary of cell counts in Chrna2-Cre+ and control mice injected with helper virus + rabies virus: including the number of incubation days after injections, the location of the injections based on scar tissue and/or location of starter cells (average coordinate and standard deviation), number of starter cells (GFP+ and mCherry+), number of traced cells (mCherry+), and the coordinates of the anteroposterior spread of the traced cortical cells.

Animal: Genotype ID	Days virus incubation	Location of injection relative to bregma (mm)	Number of starter cells	Number of traced cells	Location of traced cortical cells relative to bregma (mm)
Chrna2-Cre+ 66220	7 + 10	0.86 Cortical scar tissue	0	761	+2.34 to −1.34
Chrna2-Cre+ 66223	7 + 7	1.30 (SD 0.17) Starter cells	15	1066	+2.85 to −1.35
Chrna2-Cre+ 66225	7 + 7	1.42 (SD 0.20) Starter cells	12	564	+2.58 to −0.22
Chrna2Cre-EGFP+ 66780	7 + 9	1.13 (SD 0.03) Starter cells	6	819	+2.10 to −1.05
Control 66130	7 + 7	1.18 Cortical scar tissue	0	4	+1.18
Control 66222	7 + 7	1.34 Cortical scar tissue	0	0	x
Control 66224	7 + 7	1.34 Cortical scar tissue	0	1	+1.34
Control 66390	7 + 7	0.80 Cortical scar tissue	0	0	x
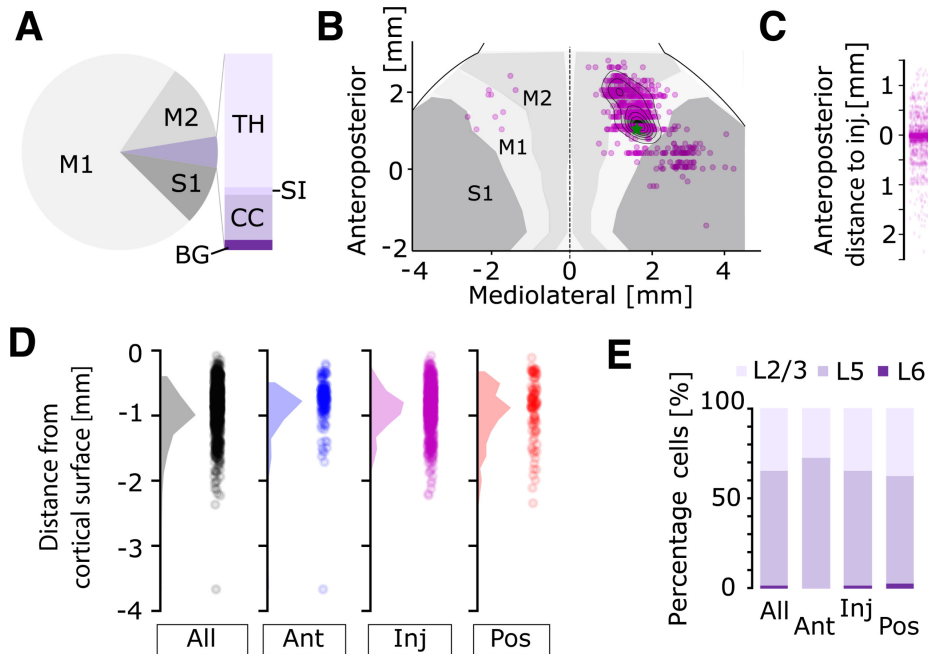
FIGURE 2 | Spatial analysis of inputs to M$^{\alpha 2}$ cells. (A) Distribution pie-chart of presynaptic inputs of Chrna2-Cre+ cells. M2, secondary motor cortex; S1, primary somatosensory cortex; TH, thalamus; CC, contralateral cortex; SI, substantia innominata; BG, basal ganglia (globus pallidus externa and striatum). (B) Density plot of the cortical traced cells in one mouse. Coordinates relative to bregma, injection site (green star). Cortical areas (M1, M2, S1) marked by gray shades. (C) Anteroposterior spread from the injection site of all traced cortical cells compiled from four mice. (D) Percentage of traced cells in different cortical layers at the injection site (Inj), >0.5 mm anterior of the injection site in M2 (Ant) and >1 mm posterior of the injection site in S1 (Pos) ($n = 4$ mice, $n = 1089$; 819, 173 and 97 cells, respectively). (E) Spread of traced cortical cells at different cortical depths at indicated positions.

Most presynaptic cells were located in the ipsilateral cortex (94.8%, SD 2.5), with 72.1% (SD 8.5) of the traced cells located in the ipsilateral M1, 12.9% (SD 8.7) in the ipsilateral secondary motor cortex (M2) and 9.8% (SD 2.3) in the ipsilateral primary somatosensory cortex (S1). Further, we found long-range projections, mostly from areas with neurons known to project to the M1, such as the thalamus (3.5%, SD 2.1), contralateral cortex (1.2%, SD 0.4), and the substantia innominata (0.19%, SD 0.1). We also found projection neurons in the globus pallidus externa (GPe; 0.19%, SD 0.2) and striatum (0.1%, SD 0.1; Figure 2A,B, Table 2). Within the ipsilateral S1, 74.1% (SD 10.8) of the cells were located in the forelimb area, 16.6% (SD 10.8) in the barrel field area, 6.8% (SD 10.8) in the mouth area and 2.5% (SD 3.3) in the hindlimb area.

In the cortex, the number of cells was highest near the injection site, with 61.9% of the cells being located on sections within 100 μm from the starter cells. The traced cortical cells were ranging from 1.4 mm anterior of the starter cells to 2.5 mm posterior ($n = 4$, 3210 cells, Figure 2C, Table 1). Traced cells were predominantly found in cortical layer 2/3 (34.6%) and 5 (63.5%), with no cells in layer 4 ($n = 3$ mice, 312 cells; 44 (Ant), 156 (Inj) and 112 (Post); Figure 2D). Accordingly, the traced cortical cells had a similar dorsoventral spread ($n = 2$ mice) at the injection site (819 cells) as well as anterior of the injection site (173 cells), whereas more posterior cells had a bimodal dorsoventral spread (97 cells; Figure 2D). The difference in dorsoventral spread could be explained by difference in cortical architecture, as the cells at the injection site and more anterior cells were located predominantly

TABLE 2 | Distribution and number of traced cells in each brain region. Cells were found in thalamus, substantia innominata, primary somatosensory cortex, primary motor cortex, secondary motor cortex, contralateral cortex, and striatum.

| Animal ID/structure	66220	66223	66225	66780
Thalamus	49 (6.4%)	18 (1.7%)	12 (2.1%)	30 (3.7%)
Substantia innominata	3 (0.4%)	1 (0.1%)	1 (0.2%)	1 (0.1%)
Primary somatosensory cortex	88 (11.6%)	107 (10.2%)	63 (11.2%)	53 (6.5%)
Primary motor cortex	572 (75.2%)	692 (65.7)	365 (64.7%)	678 (82.8%)
Secondary motor cortex	34 (4.5%)	222 (21.1%)	111 (19.7%)	52 (6.3%)
Contralateral cortex	11 (1.4%)	11 (1.0%)	9 (1.6%)	5 (0.6%)
Globus pallidus externa	3 (0.4%)	2 (0.2%)	1 (0.2%)	0 (0.0%)
Striatum	1 (0.1%)	0 (0.0%)	2 (0.4%)	0 (0.0%)
Total	761	1053	564	819
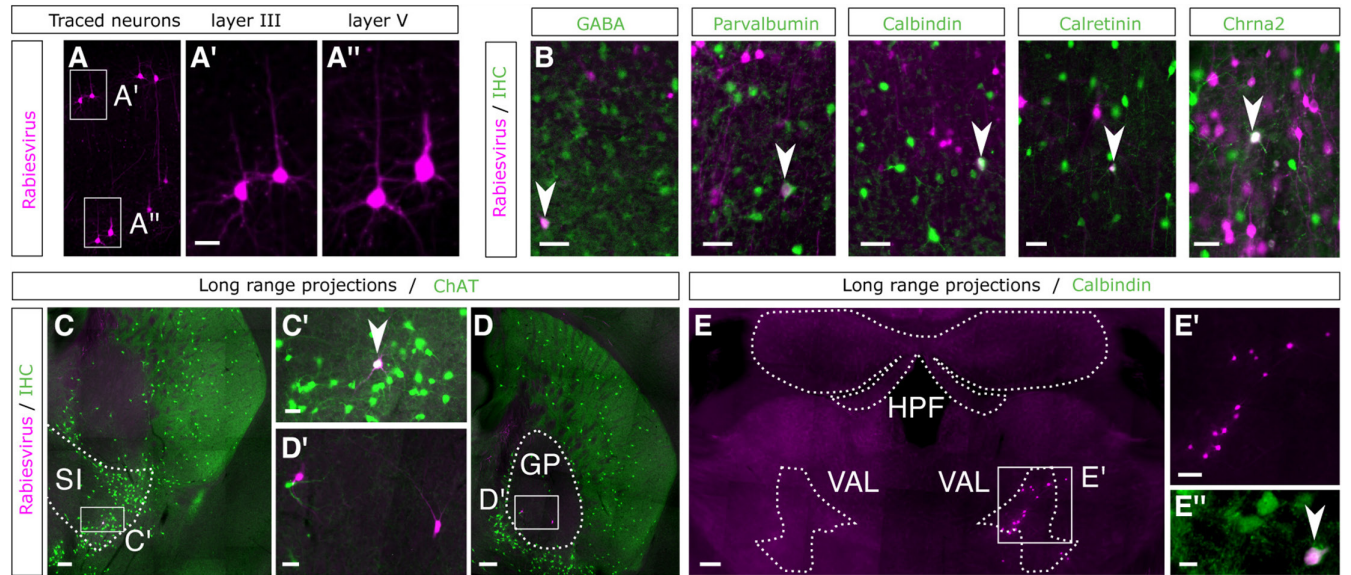
FIGURE 3 | Characterization of neurons projecting to M$^{\alpha 2}$ cells. (A) Pyramidal cells in M1 cortical layer 3 (A') and 5 (A"). (B) Immunohistochemical stainings (IHC; green) of traced cells (magenta) in the cortex around the injection site demonstrate double-positive cells of indicated antibody target (arrowheads). (C,D) Traced cell (arrowhead, magenta) in the C) ipsilateral substantia innominata and D) ipsilateral globus pallidus (SI and GP, delineated by dotted lines), with immunolabeled ChAT+ cells (green). Box indicates area of enlargement in C' and D'. (E) Traced cells in the ipsilateral ventral anterolateral complex of the thalamus (VAL). Hippocampal formation (HPF) and VAL are delineated by dotted lines. E', enlargement of the traced cells seen in E. E", a calbindin+ (green) traced cell (white, arrowhead). Scale bars: 200 μm in C, D, and E, 100 μm in E', 20 μm in E", and 40 μm in A', A", B, C', and D'.

in M1 and M2 (where layer 4 is not present), whereas the posterior cells were located mostly in S1 (Figure 2B).

Most traced cell somata had a pyramidal shape and were located in cortical layers 2/3 and 5 (Figure 3A). The identity of traced cells was analyzed using immunohistochemistry, with focus on markers commonly used to identify cortical interneurons. At the injection site, 2.5% co-expressed GABA. However, farther away than 0.5 mm from the starter cells, none of the traced cortical cells were positive for GABA. As expected, this suggested that most traced cells were excitatory, presumably PCs. We used markers for subpopulation of inhibitory interneurons to characterize the inhibitory input to $M^{\alpha 2}$ cells and found that, within 0.5 mm from the injection site, 4.2% of the traced cortical cells co-expressed PV, 0.8% calbindin and 0.4% calretinin. In the Chrna2Cre-EGFP mouse, there were seven GFP and mCherry double-positive cells, of which one was classified as a possible traced cell based on its location more than 1 mm away from the injection site (Figure 3B, Table 3), and the rest were classified as starter cells. None of the traced cortical cells expressed SST, VIP or choline acetyltransferase (ChAT).

To investigate expected cholinergic inputs, considering the cholinergic receptor genetic marker, we performed immunostainings for ChAT. We found immunopositive traced cells in substantia innominata (2/3 mCherry+ cells, Figure 3C), but no immunopositive traced cells in striatum (0/3 mCherry+ cells) or

GPe (0/9 mCherry+ cells; Figure 3D). The traced thalamic cells were found in the ipsilateral ventral anterolateral complex of the thalamus (VAL; 94.1%), anteromedial nucleus (3.3%), posterior complex (1.3%), mediodorsal nucleus (0.7%) and ventral posterolateral nucleus (0.7%). Whereas none of the immunostained traced cells in the thalamus expressed PV (0/29 cells), a small fraction expressed calbindin (3/20 cells; Figure 3E), indicating that the traced cells were excitatory principal neurons (Bjerke et al. 2021).

Previous studies have proven a role for SST interneurons in motor learning and retention of previously acquired motor skills (Adler et al. 2019; Cichon and Gan 2015; Ren et al. 2019). Based on our tracing results showing direct inputs from the thalamus and somatosensory cortex, we hypothesized that $M^{\alpha 2}$ cells might play a role in sensorimotor integration. For instance, input from the S1 forelimb area could be important for minimizing delays in sensorimotor control and adjustments of skilled forelimb movements (Franklin and Wolpert 2011). In humans, the somatosensory cortex also contributes to the initial retention of newly learnt movements (Ebrahimi and Ostry 2024). Moreover, S1 has a layer-specific projection pattern and predominantly projects to SST interneurons in cortical layer 5 of the M1, with fewer and weaker connections to SST in other cortical layers (Okoro et al. 2022). Further, activation of high-order thalamocortical inputs leads to increased PV and VIP interneuron activity and decreased SST interneuron activity, which leads to disinhibition of PCs and increased synaptic plasticity (Williams and Holtmaat 2019). To probe if $M^{\alpha 2}$ cells of the M1 might interfere with sensorimotor integration, we thus turned to chemogenetic activation (Armbruster et al. 2007), counteracting a possible disinhibition of PCs relayed by $M^{\alpha 2}$ cells. Mice injected with viral vectors carrying the modified Gq-coupled human M3 muscarinic receptor under Cre-dependent expression (Alexander et al. 2009) were tested in the hanging wire test after either saline or clozapine administration (Figure 4A,B). The hanging wire test is used to evaluate parameters such as grip strength, endurance and coordination (Ruan and Yao 2020). Since grip strength is highly dependent on sensory feedback (Witney et al. 2004), the hanging wire test can also be used to study sensorimotor integration (Bui et al. 2013). The control group, consisting of Cre-negative littermates, received the same treatment as experimental Chrna2-Cre+ mice, controlling for both Cre-independent leaky expression of the Gq receptor and off-target effects of clozapine (Figure 4C). We found an interaction effect of genotype and treatment after excitation on the number of falls during the hanging wire test (ANOVA, $F(1,12)=10.894$, $p=6.0e{-}03$), with Chrna2-Cre+ mice having more falls/min than control mice after clozapine administration ($n=7$ control and 7 Chrna2-Cre+; Tukey's HSD eff. Size = 1.656; $p=1.4e{-}02$) compared to baseline control injections in both groups (NaCl; $n=7$; t test eff. size = 1.636; $p=2.5e{-}02$; Figure 4B). By instead reducing the activity of $M^{\alpha 2}$ cells, we observed no effect of genotype, treatment or interaction ($n=7$ control and 7 Chrna2-Cre+, ANOVA-type, F1-LD-F1 model $F(1,inf)<2.64$, $p>0.104$) in the number of falls per minute (Figure 4B). Additionally, we observed no differences between clozapine and NaCl treatments for either genotype (Wilcoxon signed-rank effect size < 0.779; $p>0.079$), nor any differences between genotypes for either treatment (Mann–Whitney U effect size < 0.227; $p>0.79$). We performed post-hoc histological analysis to confirm that the spread and level of expression were comparable across the inhibitory and excitatory DREADD

TABLE 3 | Number of double-positive immunolabelled traced cortical cells for different antigens.

| Distance from injection site	Marker	Number of mCherry+ cells	Number of double-positive cells
< 0.5 mm	GABA	200	5
≥ 0.5 mm	GABA	94	0
< 0.5 mm	Parvalbumin	190	8
≥ 0.5 mm	Parvalbumin	98	0
< 0.5 mm	Somatostatin	148	0
≥ 0.5 mm	Somatostatin	24	0
< 0.5 mm	VIP	237	0
≥ 0.5 mm	VIP	20	0
< 0.5 mm	Calbindin	238	2
≥ 0.5 mm	Calbindin	59	0
< 0.5 mm	Calretinin	213	1
≥ 0.5 mm	Calretinin	17	0
< 0.5 mm	ChAT	46	0
≥ 0.5 mm	ChAT	138	0
< 0.5 mm	Chrna2	455	6 (starter cells)
≥ 0.5 mm	Chrna2	89	1
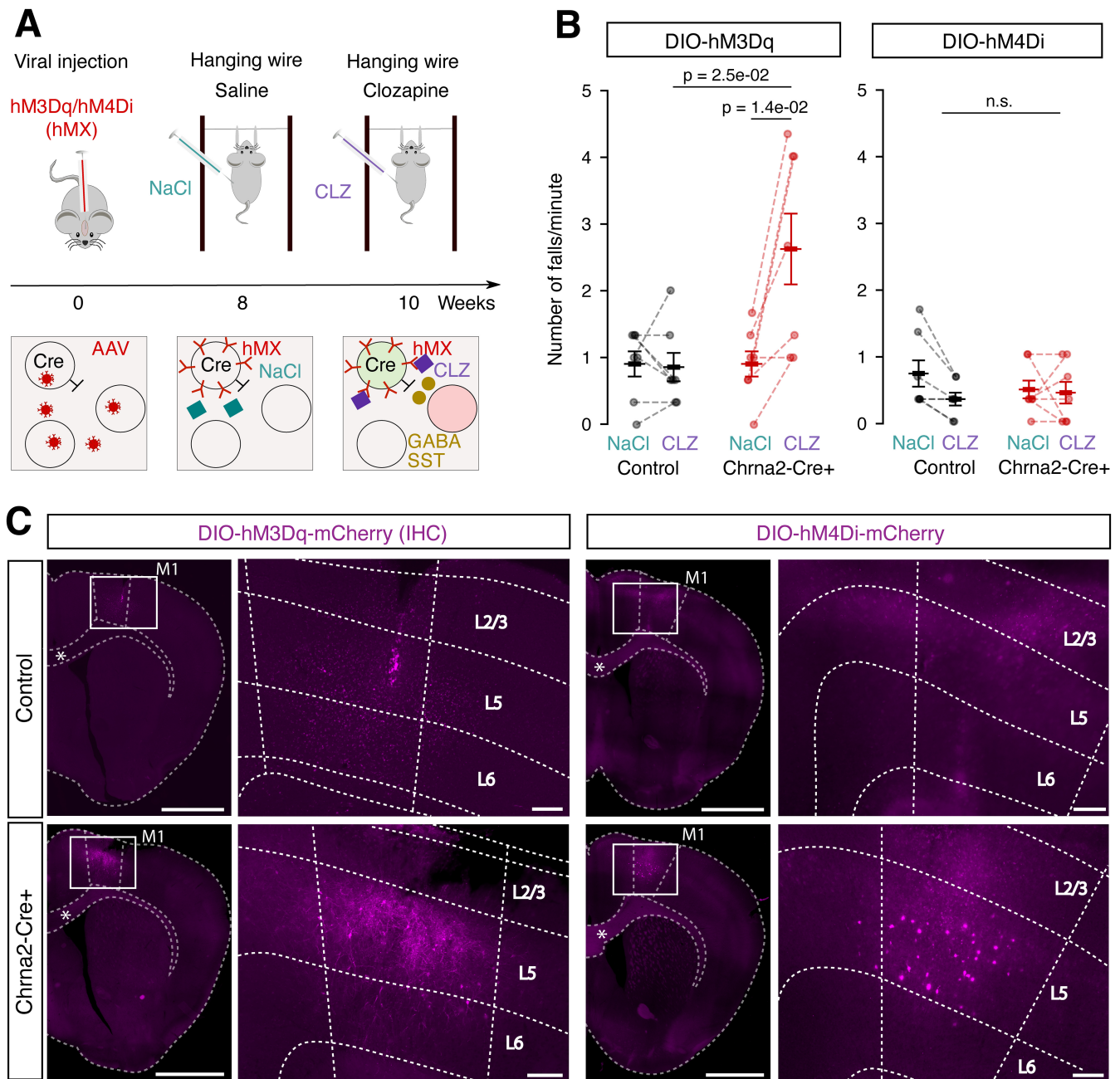
FIGURE 4 | The hanging wire test showed an increased number of falls in Chrna2-Cre+ mice upon clozapine treatment. (A) Schematic illustration of experimental timeline and method, with the adeno-associated (AAV) viral vector carrying the activating or inhibiting designer receptor exclusively activated by designer drugs (DREADDs; hM3Dq or hM4Di) injected at week 0 and the hanging wire test performed after intraperitoneal saline (NaCl) administration at week 4 (hM4Di) or 8 (hM3Dq) and after clozapine (CLZ) administration at week 5 (hM4Di) or 10 (hM3Dq). The AAV enters all cells by the injection site, and hM3Dq/hM4Di (hMX) is expressed in a Cre-dependent manner. Whereas NaCl does not affect hMX activity, CLZ binds to the receptor and increases (hM3Dq) or decreases (hM4Di) the activity of M$^{\alpha 2}$ cells (green). When activated, M$^{\alpha 2}$ cells release GABA and somatostatin (SST), inhibiting post-synaptic cells (red). (B) Graph showing the results from the hanging wire test after either hM3Dq or hM4Di injection ($n = 7$ Chrna2-Cre; $n = 7$ control mice). (C) Images of sections from brains injected to validate the expression and location of the virus expressing hM3Dq and hM4Di in Chrna2-cre+ and control (cre-) mice. Viral hM3Dq-mCherry expression was enhanced by immunohistochemistry (magenta) whereas viral hM4Di-mCherry expression was assessed by direct fluorescence (magenta). Anatomical subdivisions are mapped according to Allen Mouse Brain Atlas, mouse.brain-map.org and atlas.brain-map.org. *, corpus callosum; M1, primary motor cortex. Scale bars 500 μm (overview images), 50 μm (close up images).

experiments, which demonstrated that viral expression was specific to layer 5 cells in the M1 (Figure 4C). Together, these results suggest that increased, but not decreased, activity of M$^{\alpha 2}$ cells can interfere with grip strength and coordination.

4 | Discussion

We found that M$^{\alpha 2}$ cells in the M1 forelimb area receive direct long-range inputs from the motor thalamus, substantia

innominata, and GPe. Further, they receive cortical input from the M1, M2, and S1 areas. Within the M1, $M^{\alpha 2}$ cells receive local input from both PCs and adjacent PV interneurons. The characterization of the traced neurons should be interpreted with caution since rabies virus infection may lead to an altered host proteome, downregulating, among others, proteins involved in calcium signaling (Behera et al. 2022; Dhingra et al. 2007; Yan et al. 2019), potentially resulting in false negative immunolabeling of traced cells. Also, some types of neurons display resistance to retrograde rabies virus infection (Albisetti et al. 2017), and retrograde viral tracers show differences in neurotropism, neurotoxicity and preference of brain regions (Sun et al. 2019). Finally, there are different viral tracers derived from different viral strains (Hagendorf and Conzelmann 2015; Reardon et al. 2016) and their genetic manipulation differs (Chatterjee et al. 2018; Miyamichi et al. 2013), affecting the risk of both false negative and false positive tracing results. To minimize the risk of unspecific tracing, we used a helper virus that expresses a mutated TVA variant; however, this also decreases the efficiency to trace certain long-range projections (Miyamichi et al. 2013). Hence, false negative tracing results cannot be excluded. Another concern regarding rabies-virus based monosynaptic tracing is obtaining false positive results due to TVA leakage and unspecific tracing (Lavin et al. 2020; Velica and Kullander 2024). Based on the low number of traced cells in our control mice, we believe that the risk of false positive results is negligible.

SST interneurons target PCs, as well as PV and VIP interneurons (Markram et al. 2004; Pfeffer et al. 2013). $M^{\alpha 2}$ cells, in contrast to other types of SST interneurons, selectively target layer 5 thick-tufted type A pyramidal tract PCs, excluding thin-tufted type B intratelencephalic PCs (Hilscher et al. 2017; Wu et al. 2023). They also seem to weakly inhibit L5/6 PV interneurons, at least in the primary visual cortex (Wu et al. 2023). Whereas the excitatory input to $M^{\alpha 2}$ cells has been investigated previously, showing that $M^{\alpha 2}$ cells receive direct input from both pyramidal tract and intratelencephalic PCs (Wu et al. 2023), the inhibitory input to $M^{\alpha 2}$ cells has not been characterized before. SST interneurons are directly inhibited by VIP (Muñoz et al. 2017; Pfeffer et al. 2013) and PV interneurons (Walker et al. 2016). However, in our characterization effort, we only found input from PV interneurons and not from VIP interneurons. With the caveat that negative results can be due to technical limitations, if $M^{\alpha 2}$ cells really do not receive VIP interneuron input, they probably have different functional properties compared to other SST interneurons. Whereas SST interneurons are known to be disinhibited by VIP interneurons (Pfeffer et al. 2013), it is instead a possibility that $M^{\alpha 2}$ cells are disinhibited by PV interneurons (Walker et al. 2016).

There are several differences in long-range connectivity, comparing our tracing results with previous studies investigating the input to SST interneurons (Okoro et al. 2022). First, we found cholinergic inputs from substantia innominata of the basal forebrain, which has not been shown for SST interneurons of the M1 forelimb area (Okoro et al. 2022) nor for $M^{\alpha 2}$ cells of the S1 forelimb area or the primary visual cortex (Wu et al. 2023). This might be explained by methodological differences, such as viral tracers used or detection thresholds set for analysis. However,

cholinergic inputs from the basal forebrain are known to induce lateral inhibition via nicotinergic depolarization of Martinotti cells (Obermayer et al. 2018), which can cause decorrelation between neurons (Chen et al. 2015), enhance cortical coding (Goard and Dan 2009) and influence motor learning and acquisition of learnt motor skills (Ren et al. 2022). Lesion of the basal forebrain cholinergic system impairs motor learning and abolishes the cortical plasticity associated with motor learning (Conner et al. 2003). Moreover, artificially enhanced cholinergic modulation of SST interneurons can increase plasticity in the visual cortex and the effect is dependent on the presence of Chrna2 (Sadahiro et al. 2020). Hence, although the cholinergic inputs observed were scarce, $M^{\alpha 2}$ cells may well play an important role in cholinergic modulation of cortical plasticity.

Second, the thalamic input to $M^{\alpha 2}$ cells seems more uniform compared to the thalamic input to SST and PV interneurons. Whereas only 3.5% of the inputs to $M^{\alpha 2}$ cells were from the thalamus, 20% of the inputs to SST and PV interneurons of the M1 forelimb area are thalamic. Moreover, $M^{\alpha 2}$ cells received input primarily from one motor thalamic nucleus, the VAL, whereas SST interneurons receive input from several thalamic nuclei, with most of their input originating from sensory nuclei; the ventral posterolateral, ventral posteromedial, and posterior nucleus (Okoro et al. 2022). Furthermore, the posterior nucleus primarily targets SST interneurons in cortical layer 2/3 of the M1 (Okoro et al. 2022). Although the implication of this finding is still ambiguous, it highlights the need for a more thorough investigation of circuits guided by the cortical layer and the subtype, since interneuron populations that receive input from different long-range structures are likely to have different roles. For instance, VAL is the major nucleus projecting to M1 (Terashima et al. 1987) and neurons in the VAL form monosynaptic contacts with layer 5 PCs (Hooks et al. 2013) as well as SST and PV interneurons across layers 2–6 (Okoro et al. 2022). The cerebellum and the basal ganglia, two key motor structures involved in tuning of movements, provide feedback signals to the cortex via the thalamus (Houk and Wise 1995; Middleton and Strick 2000). The part of the motor thalamus that receives basal ganglia input projects most of its axons to layer 1 in the motor cortex, whereas the part that receives cerebellar input projects mainly to layers 3–5 (Arbuthnott et al. 1990; Kuramoto et al. 2009, 2015; Rubio-Garrido et al. 2009; Shigematsu et al. 2016). Therefore, it is possible that the information being relayed from the thalamus to $M^{\alpha 2}$ cells in the M1, which have dendrites in deeper cortical layers, originates from the cerebellum, the main target of proprioceptive signals important for coordinating purposeful movements (Tuthill and Azim 2018). The thalamocortical pathway relaying cerebellar information to the M1 via VAL is also important for initiation of sensory-triggered motor actions (Dacre et al. 2021).

Third, whereas $M^{\alpha 2}$ cells of the M1 received input from GPe, $M^{\alpha 2}$ cells of the S1 and the primary visual cortex did not receive input from GPe (Wu et al. 2023), illustrating that $M^{\alpha 2}$ cells in different cortical areas receive long-range input from different type of structures. Further studies are needed to elucidate if there is a common denominator of $M^{\alpha 2}$ cells, in connectivity and function, across cortical areas. Regarding the GPe input, there is a known hyper direct connection from GPe to the frontal cortex in both rodents and primates (Abecassis et al. 2020; Dong et al. 2021; Okoro et al. 2022; Saunders et al. 2015), and it is

likely that such connections are also present in humans (Zheng and Monti 2022). Since none of the traced neurons in GPe were ChAT+, they are most likely inhibitory and spontaneously active (Dong et al. 2021; Saunders et al. 2015), providing tonic inhibition onto $M^{\alpha 2}$cells. The existence of a hyper direct projection from the striatum to the cortex is less studied, but it has been reported previously for SST interneurons (Okoro et al. 2022). This challenges the traditional view of basal ganglia-cortical communication and warrants further studies. Although the role of the hyper direct pathway from GPe and striatum to $M^{\alpha 2}$ cells of the M1 remains to be investigated, input from the basal ganglia has been shown to play a role in motor learning and sensorimotor control (Mirzaei et al. 2017).

Functionally, we observed an increased number of falls in the Hanging wire test, which is used to evaluate grip strength and coordination, when increasing the activity of $M^{\alpha 2}$ cells in the M1. In contrast, we did not observe any effect on the number of falls when decreasing the activity of $M^{\alpha 2}$ cells, suggesting that pyramidal tract PCs are less sensitive to reduced inhibitory input from $M^{\alpha 2}$ cells, at least for grip strength and coordination. The predictive timing and coordination of isometric grip force is highly dependent on proprioception, somatosensory feedback (Johansson 2007; Johansson et al. 1992; Johansson and Westling 1984), cerebellar input (Manto et al. 2012), and adequate basal ganglia function (Prodoehl et al. 2009; Roberts et al. 2015). Hence, $M^{\alpha 2}$ cell activation can interfere with muscle control and function, possibly through disrupted long-range proprioceptive and cutaneous feedback signals. Chrna2 interneurons have been suggested to provide tonic inhibition onto principal cells (Hilscher et al. 2023). Further, it has been proposed that local disinhibition of PCs, relayed by decreased activity of SST interneurons, enables selective patterns of activity to propagate through the cortex (Karnani et al. 2016). Thus, decreased activity of $M^{\alpha 2}$ cells, relayed by inhibition from local PV interneurons or GPe projection neurons, might be required for disinhibition of PC dendrites and adequate sensorimotor integration. Chemogenetically increased activity of $M^{\alpha 2}$ cells may distort the disinhibitory circuit, leading to inadequate sensorimotor integration and ultimately to a reduced grip strength and coordination.

To conclude, $M^{\alpha 2}$ cells were found to receive input from local PV interneurons and PCs, as well as several distant brain structures involved in sensorimotor integration. Additionally, chemogenetically increased activation of $M^{\alpha 2}$ cells decreased grip strength or coordination, potentially through disrupted sensory feedback signals. Based on these results, we propose that $M^{\alpha 2}$ cells in the M1 are involved in sensorimotor integration. Further studies are needed to understand the role of $M^{\alpha 2}$ cells in cortical circuits, and to investigate their precise functional role for sensorimotor processing in the M1.

Author Contributions

Methodology (AV), data curation (AV, IN, EA, KH, BC), validation (AV), formal analysis (AV, TM, KH), visualization (AV, KH, TM), original draft preparation (AV, KK), conceptualization (KK, AV), funding acquisition (KK, TM), writing—reviewing and editing (AV, KH, KK).

Conflicts of Interest

The authors declare no conflicts of interest.

Data Availability Statement

Data supporting the findings of this study are available from the corresponding author upon reasonable request.

Peer Review

The peer review history for this article is available at https://www.webofscience.com/api/gateway/wos/peer-review/10.1111/ejn.70086.

References

Abecassis, Z. A., B. L. Berceau, P. H. Win, et al. 2020. "Npas1 + -Nkx2.1 + Neurons Are an Integral Part of the Cortico-Pallido-Cortical Loop." *Journal of Neuroscience* 40, no. 4: 743–768. https://doi.org/10.1523/JNEUROSCI.1199–19.2019.

Adler, A., R. Zhao, M. E. Shin, R. Yasuda, and W.-B. Gan. 2019. "Somatostatin-Expressing Interneurons Enable and Maintain Learning-Dependent Sequential Activation of Pyramidal Neurons." *Neuron* 102, no. 1: 202–216.e7. https://doi.org/10.1016/j.neuron.2019.01.036.

Albisetti, G. W., A. Ghanem, E. Foster, K.-K. Conzelmann, H. U. Zeilhofer, and H. Wildner. 2017. "Identification of Two Classes of Somatosensory Neurons That Display Resistance to Retrograde Infection by Rabies Virus." *Journal of Neuroscience: The Official Journal of the Society for Neuroscience* 37, no. 43: 10358–10371. https://doi.org/10.1523/JNEUROSCI.1277–17.2017.

Alexander, G. M., S. C. Rogan, A. I. Abbas, et al. 2009. "Remote Control of Neuronal Activity in Transgenic Mice Expressing Evolved G Protein-Coupled Receptors." *Neuron* 63, no. 1: 27–39. https://doi.org/10.1016/j.neuron.2009.06.014.

Arbuthnott, G. W., N. K. MacLeod, D. J. Maxwell, and A. K. Wright. 1990. "Distribution and Synaptic Contacts of the Cortical Terminals Arising From Neurons in the rat Ventromedial Thalamic Nucleus." *Neuroscience* 38, no. 1: 47–60. https://doi.org/10.1016/0306–4522(90)90373-C.

Armbruster, B. N., X. Li, M. H. Pausch, S. Herlitze, and B. L. Roth. 2007. "Evolving the Lock to Fit the Key to Create a Family of G Protein-Coupled Receptors Potently Activated by an Inert Ligand." *Proceedings of the National Academy of Sciences* 104, no. 12: 5163–5168. https://doi.org/10.1073/pnas.0700293104.

Behera, S., R. R. Reddy, K. Taunk, S. Rapole, R. R. Pharande, and A. R. Suryawanshi. 2022. "Delineation of Altered Brain Proteins Associated With Furious Rabies Virus Infection in Dogs by Quantitative Proteomics." *Journal of Proteomics* 253: 104463. https://doi.org/10.1016/j.jprot.2021.104463.

Bjerke, I. E., S. C. Yates, A. Laja, et al. 2021. "Densities and Numbers of Calbindin and Parvalbumin Positive Neurons Across the Rat and Mouse Brain." *iScience* 24, no. 1: 101906. https://doi.org/10.1016/j.isci.2020.101906.

Bui, T. V., T. Akay, O. Loubani, T. S. Hnasko, T. M. Jessell, and R. M. Brownstone. 2013. "Circuits for Grasping: Spinal dI3 Interneurons Mediate Cutaneous Control of Motor Behavior." *Neuron* 78, no. 1: 191–204. https://doi.org/10.1016/j.neuron.2013.02.007.

Chatterjee, S., H. A. Sullivan, B. J. MacLennan, et al. 2018. "Nontoxic, Double-Deletion-Mutant Rabies Viral Vectors for Retrograde Targeting of Projection Neurons." *Nature Neuroscience* 21, no. 4: 638–646. https://doi.org/10.1038/s41593-018-0091-7.

Chen, N., H. Sugihara, and M. Sur. 2015. "An Acetylcholine-Activated Microcircuit Drives Temporal Dynamics of Cortical Activity." *Nature Neuroscience* 18, no. 6: 892–902. https://doi.org/10.1038/nn.4002.

Cichon, J., and W. B. Gan. 2015. "Branch-Specific Dendritic Ca2+ Spikes Cause Persistent Synaptic Plasticity." *Nature* 520, no. 7546: 180–185. https://doi.org/10.1038/nature14251.

Conner, J. M., A. Culberson, C. Packowski, A. A. Chiba, and M. H. Tuszynski. 2003. "Lesions of the Basal Forebrain Cholinergic System Impair Task Acquisition and Abolish Cortical Plasticity Associated With Motor Skill Learning." *Neuron* 38, no. 5: 819–829. https://doi.org/10.1016/S0896-6273(03)00288-5.

Dacre, J., M. Colligan, T. Clarke, et al. 2021. "A Cerebellar-Thalamocortical Pathway Drives Behavioral Context-Dependent Movement Initiation." *Neuron* 109, no. 14: 2326–2338.e8. https://doi.org/10.1016/j.neuron.2021.05.016.

Dhingra, V., X. Li, Y. Liu, and Z. F. Fu. 2007. "Proteomic Profiling Reveals That Rabies Virus Infection Results in Differential Expression of Host Proteins Involved in ion Homeostasis and Synaptic Physiology in the Central Nervous System." *Journal of Neurovirology* 13, no. 2: 107–117. https://doi.org/10.1080/13550280601178226.

Dong, J., S. Hawes, J. Wu, W. Le, and H. Cai. 2021. "Connectivity and Functionality of the Globus Pallidus Externa Under Normal Conditions and Parkinson's Disease." *Frontiers in Neural Circuits* 15: 645287. https://doi.org/10.3389/fncir.2021.645287.

Ebrahimi, S., and D. J. Ostry. 2024. "The Human Somatosensory Cortex Contributes to the Encoding of Newly Learned Movements." *Proceedings of the National Academy of Sciences* 121, no. 6: e2316294121. https://doi.org/10.1073/pnas.2316294121.

Franklin, D. W., and D. M. Wolpert. 2011. "Computational Mechanisms of Sensorimotor Control." *Neuron* 72, no. 3: 425–442. https://doi.org/10.1016/j.neuron.2011.10.006.

Goard, M., and Y. Dan. 2009. "Basal Forebrain Activation Enhances Cortical Coding of Natural Scenes." *Nature Neuroscience* 12, no. 11: 1444–1449. https://doi.org/10.1038/nn.2402.

Gorsuch, R. L., and C. Lehmann. 2017. "Chi-Square and F Ratio: Which Should Be Used When?" *Methods and Measurements in the Social Sciences* 8, no. 2: 58–71. https://doi.org/10.2458/v8i2.22990.

Gouwens, N. W., S. A. Sorensen, F. Baftizadeh, et al. 2020. "Integrated Morphoelectric and Transcriptomic Classification of Cortical GABAergic Cells." *Cell* 183, no. 4: 935–953.e19. https://doi.org/10.1016/j.cell.2020.09.057.

Hagendorf, N., and K.-K. Conzelmann. 2015. "Recovery of Replication-Competent and G-Gene-Deleted Rabies Viruses From cDNA." *Cold Spring Harbor Protocols* 2015, no. 12: pdb.prot089409. https://doi.org/10.1101/pdb.prot089409.

Hilscher, M. M., R. N. Leão, S. J. Edwards, K. E. Leão, and K. Kullander. 2017. "Chrna2-Martinotti Cells Synchronize Layer 5 Type a Pyramidal Cells via Rebound Excitation." *PLoS Biology* 15, no. 2: e2001392. https://doi.org/10.1371/journal.pbio.2001392.

Hilscher, M. M., S. Mikulovic, S. Perry, S. Lundberg, and K. Kullander. 2023. "The alpha2 Nicotinic Acetylcholine Receptor, a Subunit With Unique and Selective Expression in Inhibitory Interneurons Associated With Principal Cells." *Pharmacological Research* 196: 106895. https://doi.org/10.1016/j.phrs.2023.106895.

Hooks, B. M., T. Mao, D. A. Gutnisky, N. Yamawaki, K. Svoboda, and G. M. G. Shepherd. 2013. "Organization of Cortical and Thalamic Input to Pyramidal Neurons in Mouse Motor Cortex." *Journal of Neuroscience* 33, no. 2: 748–760. https://doi.org/10.1523/JNEUROSCI.4338–12.2013.

Houk, J. C., and S. P. Wise. 1995. "Feature Article: Distributed Modular Architectures Linking Basal Ganglia, Cerebellum, and Cerebral Cortex: Their Role in Planning and Controlling Action." *Cerebral Cortex* 5, no. 2: 95–110. https://doi.org/10.1093/cercor/5.2.95.

Johansson, R. S. 2007. "Sensory Input and Control of Grip." In *Novartis Foundation Symposia*, edited by G. R. Bock and J. A. Goode, 1st ed., 45–63. Wiley. https://doi.org/10.1002/9780470515563.ch4.

Johansson, R. S., C. Häger, and L. Bäckström. 1992. "Somatosensory Control of Precision Grip During Unpredictable Pulling Loads: III. Impairments During Digital Anesthesia." *Experimental Brain Research* 89, no. 1: 204–213. https://doi.org/10.1007/BF00229017.

Johansson, R. S., and G. Westling. 1984. "Roles of Glabrous Skin Receptors and Sensorimotor Memory in Automatic Control of Precision Grip When Lifting Rougher or More Slippery Objects." *Experimental Brain Research* 56, no. 3: 550–564. https://doi.org/10.1007/BF00237997.

Karnani, M. M., J. Jackson, I. Ayzenshtat, et al. 2016. "Opening Holes in the Blanket of Inhibition: Localized Lateral Disinhibition by VIP Interneurons." *Journal of Neuroscience* 36, no. 12: 3471–3480. https://doi.org/10.1523/JNEUROSCI.3646–15.2016.

Krashes, M. J., S. Koda, C. Ye, et al. 2011. "Rapid, Reversible Activation of AgRP Neurons Drives Feeding Behavior in Mice." *Journal of Clinical Investigation* 121, no. 4: 1424–1428. https://doi.org/10.1172/JCI46229.

Kuramoto, E., T. Furuta, K. C. Nakamura, T. Unzai, H. Hioki, and T. Kaneko. 2009. "Two Types of Thalamocortical Projections From the Motor Thalamic Nuclei of the rat: A Single Neuron-Tracing Study Using Viral Vectors." *Cerebral Cortex* 19, no. 9: 2065–2077. https://doi.org/10.1093/cercor/bhn231.

Kuramoto, E., S. Ohno, T. Furuta, et al. 2015. "Ventral Medial Nucleus Neurons Send Thalamocortical Afferents More Widely and More Preferentially to Layer 1 than Neurons of the Ventral Anterior–Ventral Lateral Nuclear Complex in the Rat." *Cerebral Cortex* 25, no. 1: 221–235. https://doi.org/10.1093/cercor/bht216.

Lavin, T. K., L. Jin, N. E. Lea, and I. R. Wickersham. 2020. "Monosynaptic Tracing Success Depends Critically on Helper Virus Concentrations." *Frontiers in Synaptic Neuroscience* 12: 6. https://doi.org/10.3389/fnsyn.2020.00006.

Leão, R. N., S. Mikulovic, K. E. Leão, et al. 2012. "OLM Interneurons Differentially Modulate CA3 and Entorhinal Inputs to Hippocampal CA1 Neurons." *Nature Neuroscience* 15, no. 11: 1524–1530. https://doi.org/10.1038/nn.3235.

Manto, M., J. M. Bower, A. B. Conforto, et al. 2012. "Consensus Paper: Roles of the Cerebellum in Motor Control—The Diversity of Ideas on Cerebellar Involvement in Movement." *Cerebellum* 11, no. 2: 457–487. https://doi.org/10.1007/s12311-011-0331-9.

Markram, H., M. Toledo-Rodriguez, Y. Wang, A. Gupta, G. Silberberg, and C. Wu. 2004. "Interneurons of the Neocortical Inhibitory System." *Nature Reviews Neuroscience* 5, no. 10: 793–807. https://doi.org/10.1038/nrn1519.

Middleton, F. A., and P. L. Strick. 2000. "Basal Ganglia Output and Cognition: Evidence From Anatomical, Behavioral, and Clinical Studies." *Brain and Cognition* 42, no. 2: 183–200. https://doi.org/10.1006/brcg.1999.1099.

Mirzaei, A., A. Kumar, D. Leventhal, et al. 2017. "Sensorimotor Processing in the Basal Ganglia Leads to Transient Beta Oscillations During Behavior." *Journal of Neuroscience* 37, no. 46: 11220–11232. https://doi.org/10.1523/JNEUROSCI.1289–17.2017.

Miyamichi, K., Y. Shlomai-Fuchs, M. Shu, B. C. Weissbourd, L. Luo, and A. Mizrahi. 2013. "Dissecting Local Circuits: Parvalbumin Interneurons Underlie Broad Feedback Control of Olfactory Bulb Output." *Neuron* 80, no. 5: 1232–1245. https://doi.org/10.1016/j.neuron.2013.08.027.

Muñoz, W., R. Tremblay, D. Levenstein, and B. Rudy. 2017. "Layer-Specific Modulation of Neocortical Dendritic Inhibition During Active Wakefulness." *Science* 355, no. 6328: 954–959. https://doi.org/10.1126/science.aag2599.

Noguchi, K., Y. R. Gel, E. Brunner, and F. Konietschke. 2012. "nparLD: An *R* Software Package for the Nonparametric Analysis of Longitudinal Data in Factorial Experiments." *Journal of Statistical Software* 50, no. 12: 1–23. https://doi.org/10.18637/jss.v050.i12.

Obermayer, J., T. S. Heistek, A. Kerkhofs, et al. 2018. "Lateral Inhibition by Martinotti Interneurons Is Facilitated by Cholinergic Inputs in Human and Mouse Neocortex." *Nature Communications* 9, no. 1: 4101. https://doi.org/10.1038/s41467-018-06628-w.

Okoro, S. U., R. U. Goz, B. W. Njeri, et al. 2022. "Organization of Cortical and Thalamic Input to Inhibitory Neurons in Mouse Motor Cortex." *Journal of Neuroscience* 42, no. 43: 8095–8112. https://doi.org/10.1523/JNEUROSCI.0950–22.2022.

Paxinos, G., and K. Franklin. 2012. *Paxinos and Franklin's the Mouse Brain in Stereotaxic Coordinates.* 4th ed. Academic Press.

Pfeffer, C. K., M. Xue, M. He, Z. J. Huang, and M. Scanziani. 2013. "Inhibition of Inhibition in Visual Cortex: The Logic of Connections Between Molecularly Distinct Interneurons." *Nature Neuroscience* 16, no. 8: 1068–1076. https://doi.org/10.1038/nn.3446.

Prodoehl, J., D. M. Corcos, and D. E. Vaillancourt. 2009. "Basal Ganglia Mechanisms Underlying Precision Grip Force Control." *Neuroscience & Biobehavioral Reviews* 33, no. 6: 900–908. https://doi.org/10.1016/j.neubiorev.2009.03.004.

Reardon, T. R., A. J. Murray, G. F. Turi, et al. 2016. "Rabies Virus CVS-N2c(ΔG) Strain Enhances Retrograde Synaptic Transfer and Neuronal Viability." *Neuron* 89, no. 4: 711–724. https://doi.org/10.1016/j.neuron.2016.01.004.

Ren, C., K. Peng, R. Yang, W. Liu, C. Liu, and T. Komiyama. 2022. "Global and Subtype-Specific Modulation of Cortical Inhibitory Neurons Regulated by Acetylcholine During Motor Learning." *Neuron* 110, no. 14: 2334–2350.e8. https://doi.org/10.1016/j.neuron.2022.04.031.

Ren, S. Q., Z. Li, S. Lin, M. Bergami, and S. H. Shi. 2019. "Precise Long-Range Microcircuit-to-Microcircuit Communication Connects the Frontal and Sensory Cortices in the Mammalian Brain." *Neuron* 104, no. 2: 385–401.e3. https://doi.org/10.1016/j.neuron.2019.06.028.

Riedemann, T. 2019. "Diversity and Function of Somatostatin-Expressing Interneurons in the Cerebral Cortex." *International Journal of Molecular Sciences* 20, no. 12: 2952. https://doi.org/10.3390/ijms20122952.

Roberts, H. C., H. E. Syddall, J. W. Butchart, E. L. Stack, C. Cooper, and A. A. Sayer. 2015. "The Association of Grip Strength With Severity and Duration of Parkinson's: A Cross-Sectional Study." *Neurorehabilitation and Neural Repair* 29, no. 9: 889–896. https://doi.org/10.1177/1545968315570324.

Ruan, J., and Y. Yao. 2020. "Behavioral Tests in Rodent Models of Stroke." *Brain Hemorrhages* 1, no. 4: 171–184. https://doi.org/10.1016/j.hest.2020.09.001.

Rubio-Garrido, P., F. Pérez-de-Manzo, C. Porrero, M. J. Galazo, and F. Clascá. 2009. "Thalamic Input to Distal Apical Dendrites in Neocortical Layer 1 Is Massive and Highly Convergent." *Cerebral Cortex* 19, no. 10: 2380–2395. https://doi.org/10.1093/cercor/bhn259.

Rudy, B., G. Fishell, S. Lee, and J. Hjerling-Leffler. 2011. "Three Groups of Interneurons Account for Nearly 100% of Neocortical GABAergic Neurons." *Developmental Neurobiology* 71, no. 1: 45–61. https://doi.org/10.1002/dneu.20853.

Sadahiro, M., M. P. Demars, P. Burman, P. Yevoo, A. Zimmer, and H. Morishita. 2020. "Activation of Somatostatin Interneurons by Nicotinic Modulator Lypd6 Enhances Plasticity and Functional Recovery in the Adult Mouse Visual Cortex." *Journal of Neuroscience* 40, no. 27: 5214–5227. https://doi.org/10.1523/JNEUROSCI.1373–19.2020.

Saunders, A., I. A. Oldenburg, V. K. Berezovskii, et al. 2015. "A Direct GABAergic Output From the Basal Ganglia to Frontal Cortex." *Nature* 521, no. 7550: 85–89. https://doi.org/10.1038/nature14179.

Schindelin, J., I. Arganda-Carreras, E. Frise, et al. 2012. "Fiji: An Open-Source Platform for Biological-Image Analysis." *Nature Methods* 9, no. 7: 676–682. https://doi.org/10.1038/nmeth.2019.

Shigematsu, N., Y. Ueta, A. A. Mohamed, et al. 2016. "Selective Thalamic Innervation of Rat Frontal Cortical Neurons." *Cerebral Cortex* 26, no. 6: 2689–2704. https://doi.org/10.1093/cercor/bhv124.

Sun, L., Y. Tang, K. Yan, et al. 2019. "Differences in Neurotropism and Neurotoxicity Among Retrograde Viral Tracers." *Molecular Neurodegeneration* 14, no. 1: 8. https://doi.org/10.1186/s13024-019-0308-6.

Tennant, K. A., D. L. Adkins, N. A. Donlan, et al. 2011. "The Organization of the Forelimb Representation of the C57BL/6 Mouse Motor Cortex as Defined by Intracortical Microstimulation and Cytoarchitecture." *Cerebral Cortex* 21, no. 4: 865–876. https://doi.org/10.1093/cercor/bhq159.

Terashima, T., K. Inoue, Y. Inoue, and K. Mikoshiba. 1987. "Thalamic Connectivity of the Primary Motor Cortex of Normal and Reeler Mutant Mice." *Journal of Comparative Neurology* 257, no. 3: 405–421. https://doi.org/10.1002/cne.902570309.

Tremblay, R., S. Lee, and B. Rudy. 2016. "GABAergic Interneurons in the Neocortex: From Cellular Properties to Circuits." *Neuron* 91, no. 2: 260–292. https://doi.org/10.1016/j.neuron.2016.06.033.

Tuthill, J. C., and E. Azim. 2018. "Proprioception." *Current Biology* 28, no. 5: R194–R203. https://doi.org/10.1016/j.cub.2018.01.064.

Velica, A., and K. Kullander. 2024. "A Flowchart for Adequate Controls in Virus-Based Monosynaptic Tracing Experiments Identified Cre-Independent Leakage of the TVA Receptor in RΦGT Mice." *BMC Neuroscience* 25, no. 1: 9. https://doi.org/10.1186/s12868-024-00848-1.

Walker, F., M. Möck, M. Feyerabend, et al. 2016. "Parvalbumin- and Vasoactive Intestinal Polypeptide-Expressing Neocortical Interneurons Impose Differential Inhibition on Martinotti Cells." *Nature Communications* 7, no. 1: 13664. https://doi.org/10.1038/ncomms13664.

Wang, X., Y. Liu, X. Li, et al. 2017. "Deconstruction of Corticospinal Circuits for Goal-Directed Motor Skills." *Cell* 171, no. 2: 440–455.e14. https://doi.org/10.1016/j.cell.2017.08.014.

Wang, Y., M. Toledo-Rodriguez, A. Gupta, et al. 2004. "Anatomical, Physiological and Molecular Properties of Martinotti Cells in the Somatosensory Cortex of the Juvenile Rat: Martinotti Cells in Somatosensory Cortex." *Journal of Physiology* 561, no. 1: 65–90. https://doi.org/10.1113/jphysiol.2004.073353.

Wickersham, I. R., D. C. Lyon, R. J. O. Barnard, et al. 2007. "Monosynaptic Restriction of Transsynaptic Tracing From Single, Genetically Targeted Neurons." *Neuron* 53, no. 5: 639–647. https://doi.org/10.1016/j.neuron.2007.01.033.

Williams, L. E., and A. Holtmaat. 2019. "Higher-Order Thalamocortical Inputs Gate Synaptic Long-Term Potentiation via Disinhibition." *Neuron* 101, no. 1: 91–102.e4. https://doi.org/10.1016/j.neuron.2018.10.049.

Witney, A. G., A. Wing, J.-L. Thonnard, and A. M. Smith. 2004. "The Cutaneous Contribution to Adaptive Precision Grip." *Trends in*

Neurosciences 27, no. 10: 637–643. https://doi.org/10.1016/j.tins.2004.08.006.

Wu, S. J., E. Sevier, D. Dwivedi, et al. 2023. "Cortical Somatostatin Interneuron Subtypes Form Cell-Type-Specific Circuits." *Neuron* 111, no. 17: 2675–2692.e9. https://doi.org/10.1016/j.neuron.2023.05.032.

Xu, H., H.-Y. Jeong, R. Tremblay, and B. Rudy. 2013. "Neocortical Somatostatin-Expressing GABAergic Interneurons Disinhibit the Thalamorecipient Layer 4." *Neuron* 77, no. 1: 155–167. https://doi.org/10.1016/j.neuron.2012.11.004.

Yan, W., R. Xiang, J. Chen, et al. 2019. "Proteomics Analysis of Suckling Mouse Brain Infected With Attenuated Rabies Virus Strain SRV9." *Acta Virologica* 63, no. 4: 423–432. https://doi.org/10.4149/av_2019_406.

Yavorska, I., and M. Wehr. 2016. "Somatostatin-Expressing Inhibitory Interneurons in Cortical Circuits." *Frontiers in Neural Circuits* 10: 1–18. https://doi.org/10.3389/fncir.2016.00076.

Zheng, Z. S., and M. M. Monti. 2022. "Cortical and Thalamic Connections of the Human Globus Pallidus: Implications for Disorders of Consciousness." *Frontiers in Neuroanatomy* 16: 960439. https://doi.org/10.3389/fnana.2022.960439.